

# On the Origin of Altered Diastereomeric Ratios for Anionic versus Neutral Reaction Conditions in the Oxy-Cope/Ene Reaction: An Interplay of Experiment and Computational Modeling

James Hooper, Effiette L. O. Sauer, Steve Arns, Tom K. Woo,\* and Louis Barriault\*[a]

**Abstract:** We report herein a detailed investigation into the reaction mechanism for a sequential oxy-Cope/ene reaction under anionic conditions. With DFT calculations and ab initio molecular dynamics simulations, the observed diastereoselectivity is shown to be the result of an isomerization of the enolate olefin, which would evidently not

occur under neutral conditions. The potential energy surface was thoroughly mapped out for the reaction pathways and the proposed mechanism con-

**Keywords:** carbanions • cascade reaction • decalin • ene reaction • isomerization • oxy-Cope reaction

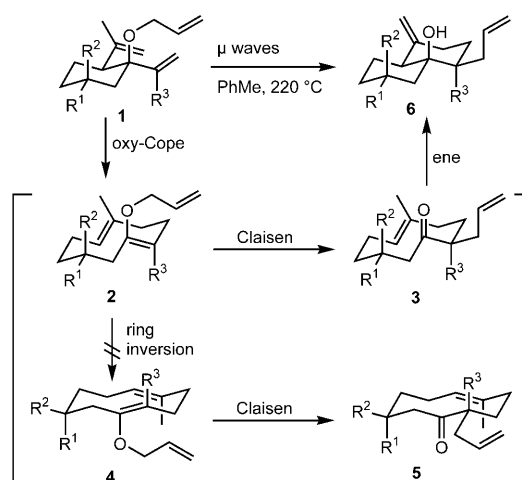
firmed the different product distributions observed under neutral and anionic oxy-Cope conditions. In addition, other possible pathways are shown to be higher in energy and experimental evidence is given that supports the olefin-isomerization pathway.

## Introduction

Recently, we reported an extensive theoretical evaluation of the reaction mechanism of a previously developed highly diastereoselective tandem oxy-Cope/Claisen/ene reaction (Scheme 1).<sup>[1]</sup> This reaction represents an efficient means of generating decalin skeletons **6** which possess multiple contiguous stereocenters and could further be functionalized to synthesize natural products.<sup>[2]</sup> From the observed conservation of enantiomeric excess and subsequent transition state free energies obtained at the DFT level of theory, we concluded the highly diastereoselective nature of the reaction was a direct result of 1) the high energy barrier to rotate the enol ether moiety (**2** to **4**) thereby favoring the formation of **3** over **5**, and 2) the product ratios resulting from a transan-

nular ene reaction (**3** to **6**) were shown to be under Curtin-Hammett control.

In further, more recent developments, it was observed that the product distributions from the oxy-Cope/ene reactions changed under different reaction conditions (Scheme 2). Heating of **7a** at 220 °C in degassed toluene and in the absence of base gave decalins **14a** and **15a** in a ratio of 7:1 [Eq. (1)], as expected from our previous study.<sup>[3]</sup> However, when the reaction was repeated in the presence of DBU (10 equivalents), isomers **14a** and **15a** were isolated

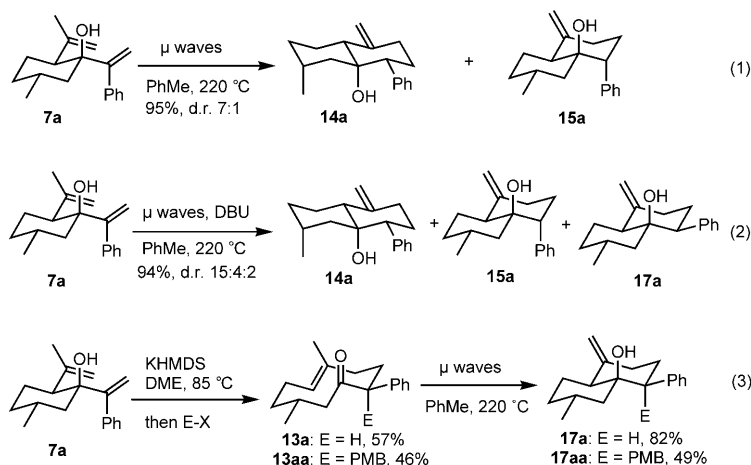


Scheme 1. Domino oxy-Cope/Claisen/ene reaction.

[a] J. Hooper, E. L. O. Sauer, S. Arns, Prof. T. K. Woo, Prof. L. Barriault  
Centre for Catalysis Research and Innovation  
Department of Chemistry  
University of Ottawa, 10 Marie Curie  
Ottawa K1N 6N5 ON (Canada)  
Fax: (+1) 613-562-5170  
E-mail: twoo@uottawa.ca  
lbarriau@uottawa.ca

Supporting information for this article is available on the WWW under <http://dx.doi.org/10.1002/chem.201001302>. It includes the Cartesian coordinates of **7**, **8**, **9**, **18**, **19**, **20**, **21**, and **22** and all the relevant transition states in Scheme 6. <sup>1</sup>H and <sup>13</sup>C NMR spectra of **13a**, **13d**, **14a**, **15a**, **17a**, and **17aa** are also given.

along with a third product **17a** in a 15:4:2 ratio [Eq. (2)]. Under anionic conditions, oxy-Cope rearrangement of **7a**<sup>[4]</sup> followed by the addition of E–X afforded macrocycles **13a** and **13aa** which upon heating led to **17a** and **17aa** respectively as the sole observable isomers [Eq. (3)].



Scheme 2. Anionic versus neutral reaction conditions.

Considering these variable product distributions, as shown in Scheme 2, it becomes clear that the current mechanistic picture is problematic for the reaction of these substrates under anionic conditions (Scheme 3). The diastereoselectivity from reacting **7** under anionic oxy-Cope conditions requires not only that the ring inversion of **8'** to **9'** is fast and low in energy, but also that the protonation or alkylation of **9'** occurs exclusively over that of **8'** (Scheme 3). It is this latter condition that is especially difficult to reconcile. Herein we will use the labeling convention where an enol-enolate pair will be given the same structure number, but the enolate will be primed. In this article, we present extensive DFT and ab-initio molecular dynamics calculations and report an olefin isomerization reaction mechanism which explains the diastereomeric ratios observed under different oxy-Cope/ene conditions. Experimental evidence in support of the new mechanism is provided.

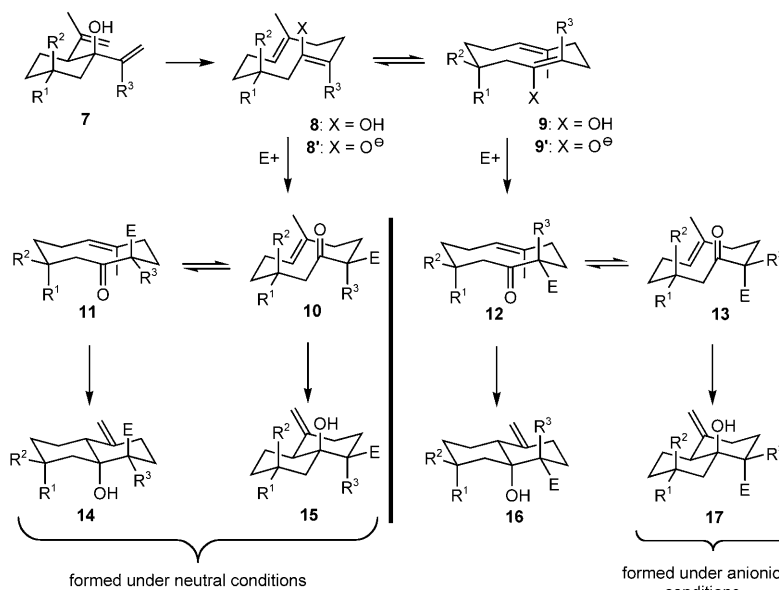
## Methods

For geometry optimizations of all reactants, products, intermediates, and transition states, Kohn–Sham DFT<sup>[5]</sup> calculations were performed with the hybrid B3LYP exchange functional<sup>[6]</sup> using a 6-311++G\*\* Pople basis set

within the ab initio electronic structure package Jaguar.<sup>[7]</sup> Frequency calculations were used to confirm the nature of all local minima and saddle points on the potential energy surface. In cases where visual inspection of the imaginary modes in transition states did not suffice, intrinsic reaction coordinate (IRC) calculations were used to confirm that all transition states lie between the desired reactants and products.

The ten-membered ring structural motif present in most of the molecules in this study makes for a large degree of conformational flexibility. The default Monte-Carlo based conformational search engine of the Spartan 2002 molecular modeling package<sup>[8]</sup> was therefore used to carry out a conformer search on the backbone of the ring at the semi-empirical, PM3,<sup>[9]</sup> level of theory to ensure that the lowest energy local minima/transition states were found. The effects of solvents on the energy profile of the presented reaction mechanisms were quantified using a polarizable continuum model (PCM) as implemented in Jaguar.<sup>[10]</sup> In the solvent calculations a probe radius of 2.75 Å was used with a dielectric constant of 10 and the geometries were reoptimized within the solvent model. Ab initio molecular dynamics simulations were performed with the CPMD software package<sup>[11]</sup>

using the Car–Parrinello method on select molecules to explore hitherto unexplored reaction pathways. For these simulations we used the gradient-corrected PBE functional<sup>[12]</sup> and the norm-conserving Martins–Troullier pseudopotentials with the Kleinman–Bylander transformation to the fully non-local form to describe the core electronic states.<sup>[13]</sup> The Kohn–Sham orbitals were expanded in plane waves with an energy cutoff of 60 Ry and a fictitious electronic mass of 400 a.u. was employed for the dynamic evolution of the electronic structure. The integration time step was 0.12 fs and the 700 or 1100 K simulation temperatures were controlled by intermittently rescaling the velocities throughout the simulation.

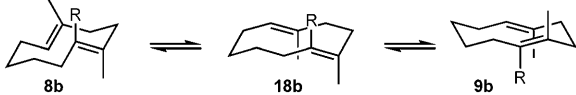


Scheme 3. General mechanism for the oxy-Cope/ene reaction.

## Results and Discussion

For the mechanism in Scheme 3 to apply to anionic conditions, the swiveling of the tetrasubstituted enolate in intermediate **8'** would have to be substantially lower in energy than that of the corresponding enol form **8**. To investigate this possibility, the relative free energy barriers for the corresponding ring inversions were calculated in the gas-phase for **8b'** and **8b** at 473 K. The results are summarized in Table 1.<sup>[14]</sup> For both the enol and enolate intermediates, the

Table 1. Relative free energies for the neutral and anionic ring inversion of **8b** and **8b'**.



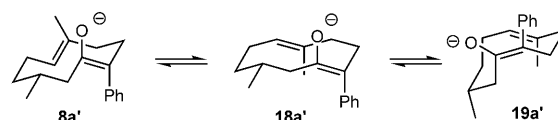
Enol (R=OH)	$\Delta G^{[a]}$ [kcal mol <sup>-1</sup> ]	Enolate (R=O <sup>-</sup> )	$\Delta G^{[a]}$ [kcal mol <sup>-1</sup> ]
<b>8b</b>	0.0	<b>8b'</b>	0.0
<b>[8b→18b]<sup>‡</sup></b>	18.9	<b>[8b'→18b']<sup>‡</sup></b>	17.5
<b>18b</b>	4.8	<b>18b'</b>	5.3
<b>[18b→9b]<sup>‡</sup></b>	88.8	<b>[18b'→9b']<sup>‡</sup></b>	80.0
<b>9b</b>	0.0	<b>9b'</b>	0.0

[a] Gas-phase relative free energies at 473 K calculated at the B3LYP/6-311G\*\* level using DFT.

first step of the ring inversion from **8b**/(**8b'**) to **18b**/(**18b'**), that is, the rotation of the trisubstituted olefin, was calculated to be relatively low in energy. Both transition states [**8b**→**18b**] and [**8b'**→**18b'**] are lower than 20 kcal mol<sup>-1</sup>. This suggests that it occurs quite readily under the reaction conditions. However, as expected from our previous studies, the second step was found to be much higher in energy.<sup>[2a]</sup> The activation energies for [**18b**→**9b**]<sup>‡</sup> and [**18b'**→**9b'**]<sup>‡</sup> are 89 and 80 kcal mol<sup>-1</sup>, respectively. Though these numbers do suggest that the inversion of the anionic intermediate is more facile than that of the neutral enol, the difference is not sufficient to explain the observed trends. The activation barrier of both processes remains quite high.

Ab initio molecular dynamics (MD) simulations can be an effective computational tool for probing reaction dynamics when the underlying potential energy surface and reaction mechanism are unclear, particularly for intramolecular reactions. In this light, a series of ab initio MD simulations were run on the intermediates **8a**, **8a'**, **9a** and **9a'**, in order to evaluate the evolution of the enolate/enol macrocycle inversion over time. The motivation was to shed light on the mechanism responsible for the altered product distributions seen from oxy-Cope/ene rearrangements of **7** under anionic versus neutral reaction conditions. High temperatures were chosen in an effort to increase the chances of observing energetically demanding transformations and are justified since we were only interested in seeing alternative reaction pathways to those we had considered thus far. In the 12 ps MD simulations of the enol species (**8a**, **9a**) and the enolate species (**8a'**, **9a'**) the ring was found to invert about the trisubstituted olefin, that is, **8a'** to **18a'** as shown in the first

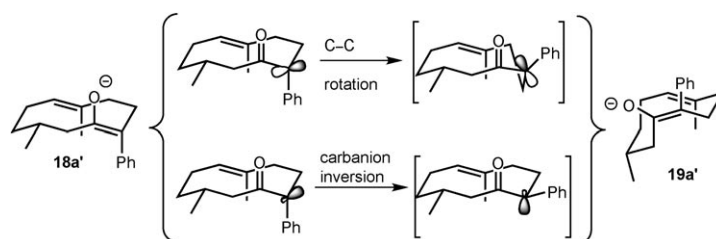
part of Scheme 4. This inversion was expected, and through our previously discussed static calculations we found this process to have a modest barrier of about 18 kcal mol<sup>-1</sup>. In the MD simulations of **8a**, **9a**, and **9a'** this ring inversion was observed several times during the course of the dynamics. However, for the simulation of the enolate, **8a'**, after an initial ring inversion to **18a'** that occurs after 1 ps, an unforeseen transformation occurs. At around the 2 ps mark of the simulation **18a'** isomerizes to **19a'** as shown in Scheme 4.



Scheme 4. Isomerization of enolate **8a'** observed during an ab initio molecular dynamics simulation.

Analysis of the MD trajectory provides some insight into the nature of the observed isomerization. The conversion of **18a'** to **19a'** involves an *E* to *Z* isomerization about the olefinic C1–C2 bond as labeled in Figure 1 a. This isomerization can be characterized by the Cp–C2–C1–O torsion angle of the enolate and this torsion's evolution over the course of the MD simulation is plotted in Figure 1 b. Figure 1 b shows that the torsion angle initially fluctuates around 150°, which is indicative of the *E* conformer of the olefin. At the 2 ps point of the simulation the torsion angle rapidly decreases to an average value of ~0°, which characterizes the *Z* isomer. For the remainder of the simulation, the enolate remains in the *Z* isomer.

Normally, double bond character in the C–C bond of an enolate prevents this type of isomerization from occurring. The observed change in geometry suggests that enolate **18a'** possesses carbanion character with a C1–C2 single bond. An NBO analysis<sup>[15]</sup> provides a C1–C2 bond order of 1.35 in **18a'**, which is lower than the calculated 1.73 bond order in the corresponding enol **18a**. The isomerization process could then be the result of either a simple rotation about the C–C enolate bond or a pyramidal carbanion inversion as depicted in Scheme 5.<sup>[16]</sup> From a visual inspection of the molecular dynamics simulations alone, it is not obvious which process is responsible for the interconversion of **18a'** to **19a'**. A carbanion inversion would imply that the trigonal



Scheme 5. Possible modes of enolate isomerization: rotation versus inversion.

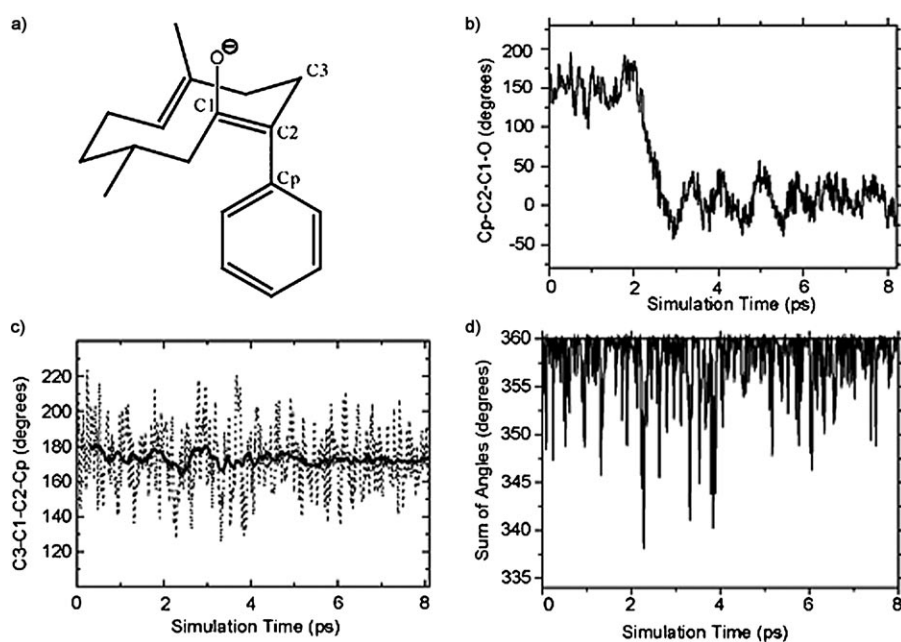


Figure 1. a) **8a'** shown with labeled atoms. b) Evolution of the Cp-C2-C1-O dihedral angle, c) evolution of the C3-C1-C2-Cp improper dihedral angle (dotted line) and its running average over 600 fs time steps (solid line), and d) evolution of the sum of the C1-C2-Cp, Cp-C2-C3, and C1-C2-C3 bond angles during an ab initio molecular dynamics simulation initiated from structure **8a'**.

pyramidal C2-carbon goes through a trigonal planar transition state as the geometry inverts; a simple bond rotation would not. Figure 1c shows the evolution of an improper dihedral angle that measures the planarity of the tricoordinated C2 center throughout the simulation. An improper torsion angle of 180° in Figure 1c corresponds to a trigonal planar  $\beta$ -carbon, while tetrahedral-like coordination would be closer to 120°. The plot in Figure 1c shows that throughout the isomerization, the geometry oscillates about a near trigonal planar geometry with the improper dihedral averaging  $\sim 170^\circ$  throughout the simulation. The absence of an obvious change in planarity before and after the isomerization suggests the transformation is best characterized as a bond rotation. Additional insight can be gained by examining the sum of the three bond angles involving C2 as the central atom. Since carbanions typically have puckered geometries with tetrahedral-like bond angles around 109° and  $sp^2$ -hybridized carbons are trigonal planar near 120°, the sum of the three bond angles should change during the isomerization if a carbanion inversion is involved. Specifically, a carbanion would have bond angles totaling  $\sim 327^\circ$  while those of a trigonal planar transition state should total  $\sim 360^\circ$ . Figure 1d shows that the sum of angles remains close to the maximum of 360° throughout, although there are transient spikes that can be attributed to the high temperature vibrations.

To further explore this mechanism, a static transition state was located by scanning the dihedral angle between the enolate oxygen and the phenyl group. The isomerization transition state,  $[18a' \rightarrow 19a']^\ddagger$ , is shown in Figure 2 and, importantly, was found to have an activation barrier of only

$19.7 \text{ kcal mol}^{-1}$  relative to **18a'**. From inspection of the imaginary vibrational mode in the transition state, we could not clearly distinguish between an inversion or rotation process because of the concerted motions of the ring. However, if a carbanion inversion were taking place, the C2 center in **18a'** should be initially puckered, becoming more trigonal planar as it passes through the transition state. In this case, the opposite is found. Specifically, the C3-C1-C2-Cp improper torsion is found to be 178° in **18a'** while it decreases in the transition state to 166° and then increases again to 177° in **19a'**. An IRC calculation was performed to confirm this pathway. Thus, both a static potential energy scan and the MD simulations suggest that

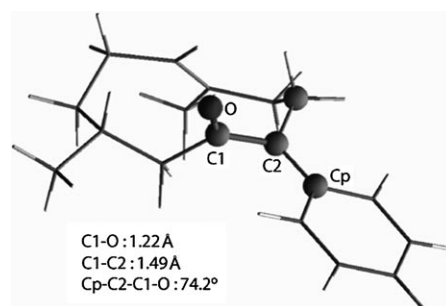
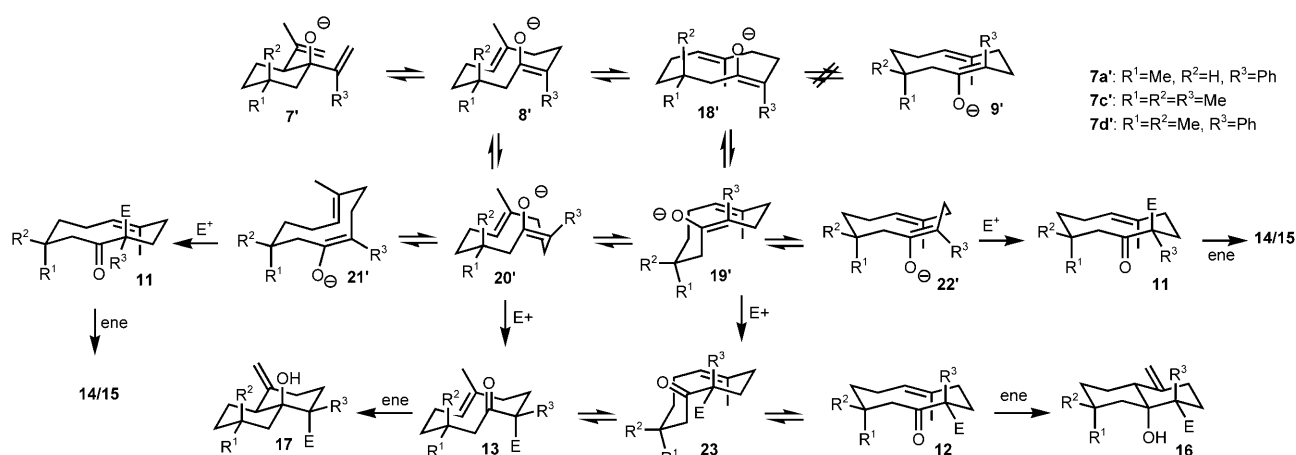


Figure 2. Calculated transition state for enolate isomerization of **18a'**.

the isomerization from **18a'** to **19a'** can best be characterized as a bond rotation about the enolate carbon-carbon bond.

Incorporation of the *Z* to *E* enolate isomerization leads to a new proposed reaction mechanism for the oxy-Cope/ene reaction under anionic conditions (Scheme 6). To assess the feasibility of the overall pathway, we evaluated the relative Gibbs free energies of the transition states and intermediates for three substrates **7a'**, **7c'** ( $R^1 = R^2 = R^3 = \text{Me}$ ), and **7d'** ( $R^1 = R^2 = \text{Me}$  and  $R^3 = \text{Ph}$ ) as shown in Table 2. For all three substrates, the transition state energy for the second step of the ring inversion  $[18' \rightarrow 9']^\ddagger$  (entries 4–6) is over twice as high as that of the olefin isomerization transition states  $[8' \rightarrow 20']^\ddagger$  (entries 7–9) and  $[18' \rightarrow 19']^\ddagger$  (entries 10–12). This clearly shows that the latter process is the favored pathway. In addition to being lower in energy, this olefin isomerization mechanism predicts the establishment of an equilibrium between six intermediate enolate conformers: **8'**,



Scheme 6. New hypothesis for the anionic oxy-Cope/ene reaction mechanism.

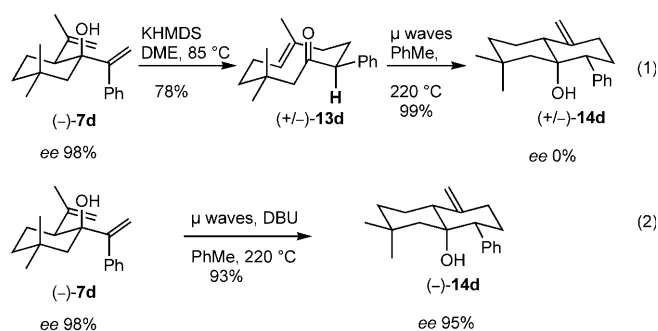
Table 2. Relative free energies for the proposed isomerization mechanism of **7**.

Entry	Transition state	$\Delta G$ [kcal mol <sup>-1</sup> ]
1	[ <b>8a'</b> → <b>18a'</b> ] <sup>‡</sup>	15.3
2	[ <b>8c'</b> → <b>18c'</b> ] <sup>‡</sup>	15.9
3	[ <b>8d'</b> → <b>18d'</b> ] <sup>‡</sup>	15.5
4	[ <b>18a'</b> → <b>9a'</b> ] <sup>‡</sup>	74.3
5	[ <b>18c'</b> → <b>9c'</b> ] <sup>‡</sup>	74.8
6	[ <b>18d'</b> → <b>9d'</b> ] <sup>‡</sup>	70.2
7	[ <b>8a'</b> → <b>20a'</b> ] <sup>‡</sup>	22.7
8	[ <b>8c'</b> → <b>20c'</b> ] <sup>‡</sup>	34.9
9	[ <b>8d'</b> → <b>20d'</b> ] <sup>‡</sup>	21.7
10	[ <b>18a'</b> → <b>19a'</b> ] <sup>‡</sup>	24.2
11	[ <b>18c'</b> → <b>19c'</b> ] <sup>‡</sup>	33.2
12	[ <b>18d'</b> → <b>19d'</b> ] <sup>‡</sup>	25.2

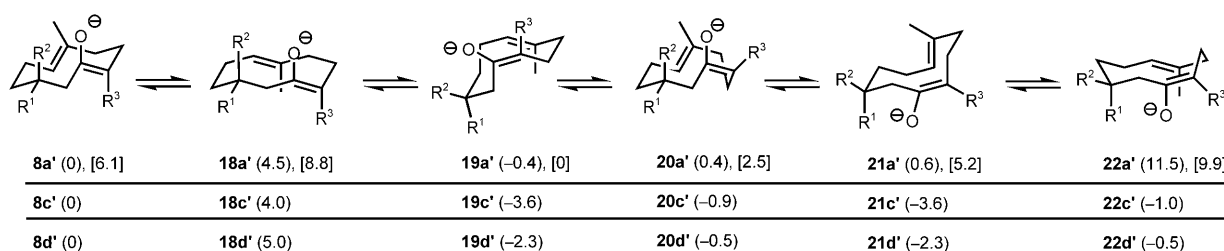
**18'**, **19'**, **20'**, **21'** and **22'** (Scheme 6). Conformers **21'** and **22'** are derived from **20'** and **19'**, respectively, by flipping the position of the enolate moiety. The relative energies of the six competing enolates are given in Scheme 7 for all three substrates.

A closer inspection of the calculations predicts that the **19c'**, **21c'**, **19d'** and **21d'** enolate structures, generated from **7c** and **7d**, respectively, should dominate their respective equilibria (Scheme 7). Since conformers **19c'** and **19d'** are mirror images of **21c'** and **21d'**, respectively, racemization is thus predicted. To validate the above hypothesis, enantiomerically pure (–)-**7d** was exposed to two sets of

oxy-Cope/ene conditions. In the first experiment, (–)-**7d** underwent an anionic oxy-Cope in the presence of KHMDS at 85 °C in THF. This was followed by a thermal ene reaction in toluene at 220 °C (Scheme 8, Eq. (1)). In a separate experiment, **7d** was directly heated at 220 °C in the sole presence of DBU [Eq. (2)]. In both cases, decalin **14d** was obtained as the product with yields of 99 and 93 % yield, respectively. Comparing the enantiomeric excess of the isolated **14d** revealed a significant difference between the two reaction conditions: under anionic conditions, complete racemization was observed [Eq. (1)] while the comparatively neutral conditions led to near retention of chirality (*ee* 95 % for **14d**) [Eq. (2)].



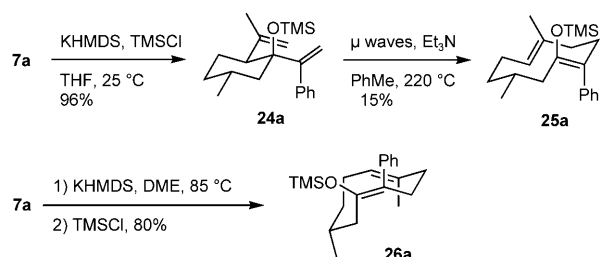
Scheme 8. Tandem oxy-Cope/ene reaction of (–)-**7d**.



Scheme 7. Relative free energies (kcal mol<sup>-1</sup>) and solvation energies [kcal mol<sup>-1</sup>] for six competing equilibrium conformers. The relative solvation free energies were evaluated with a dielectric constant = 10.

For substrate **7a**, the only experimentally observed product of the anionic oxy-Cope/ene reaction is **17a** [Scheme 2, Eq. (3)]. From the newly proposed mechanism depicted in Scheme 6, it can be seen that protonation of the lowest energy structure, **19a'** ( $-0.4 \text{ kcal mol}^{-1}$ ), gives **13a**, which, following a transannular ene reaction gives the observed product, **17a**. While the preferential formation of **17a** is rationalized by these gas-phase calculations, the  $0.4 \text{ kcal mol}^{-1}$  preference for conformer **19a'** over **8a'** is insufficient to explain the exclusive formation of **17a**. To probe this ambiguity further, solvent effects were incorporated into the electronic structure calculations using the PCM continuum model. The results from a representative set of these calculations are reported in Scheme 7. Notably, these relative solvation energies show an increased preference for **19a'** by  $>2.0 \text{ kcal mol}^{-1}$  from the  $0.4 \text{ kcal mol}^{-1}$  preference of the gas-phase free-energy profile.

As further confirmation of the proposed isomerization pathway, an additional set of experiments was carried out on substrate **7a** in the hopes of trapping the *Z* enolate (Scheme 9). In the first case, the tertiary alcohol of **7a** was



Scheme 9. Trapping the *E* and *Z* enolates.

protected with a TMS group prior to being subjected to a thermal oxy-Cope rearrangement. Silyl enol ether **25a** was isolated in 15% yield along with 75% of the unreacted starting material **24a**.<sup>[4]</sup> A series of NOE signals established a *trans* relationship between the OTMS and phenyl groups as shown, as well as the orientation of the trisubstituted double bond. In contrast, when the anionic oxy-Cope of **7a** was quenched with TMSCl, the macrocycle **26a** was found to have a *cis* geometry between the OTMS and phenyl groups. This confirms that under these reaction conditions, isomerization of the enolate olefin can and does occur.

## Conclusion

A detailed mechanistic analysis of anionic oxy-Cope/ene reaction of 1,2-divinylcyclohexanols has been presented. A combination of experimental evidence, static DFT calculations and ab initio molecular dynamics simulations revealed that the observed diastereoselectivity is the result of an isomerization rather than an inversion of the tetrasubstituted enolate through the 10-membered ring. It was demonstrated that such a process does not occur under neutral

thermal conditions. DFT calculations and DFT-based molecular dynamics simulations suggest that the isomerization proceeds through what can be best characterized as a carbocation-related bond rotation. Evaluation of this new mechanism on other macrocyclic enolates of various ring sizes is underway and the results will be reported in due course.

## Experimental Section

**General:** All reactions were performed under argon or nitrogen unless otherwise dictated by the experimental protocol. Glassware was flame-dried under high vacuum, and each reaction vessel was equipped with a rubber septum and magnetic stir bar. Solvents were typically distilled prior to use. All other solvents and chemicals were used without further purification unless otherwise noted. Microwave-accelerated reactions were performed in either a CEM Corporation MARS microwave reactor or a CEM Corporation Discover LabMate microwave reactor using a quartz reaction vessel and a Carboflon to assist in the absorption of microwaves. All microwave reactions were degassed with argon prior to heating. Reactions were monitored by TLC analysis using silica gel coated glass plates. TLC plates were developed by using UV irradiation, *p*-anisaldehyde staining solution, phosphomolybdic acid staining solution, potassium permanganate staining solution or iodine. Flash chromatography was carried out using 230–400 mesh silica gel. NMR spectra were recorded on several instruments, including Bruker AVANCE 300 and 400 MHz spectrometers, a Bruker AVANCE 500 MHz Wide Bore spectrometer and a Varian INOVA 500 MHz spectrometer. Spectra were calibrated according to standardized chemical shifts of the NMR solvent. IR spectra were recorded on a Bomen Michaelson FT-IR spectrometer. HRMS spectra were obtained on a Kratos Analytical Concept spectrometer and melting points were measured on a Gallenkamp P1106G Melting Point Apparatus.

**(±)-(4*R*,4*aR*,6*R*,8*aR*)-6-Methyl-1-methylene-4-phenyl-octahydronaphthalen-4*a*-ol (14*a*) and (±)-(4*R*,4*aS*,6*R*,8*aS*)-6-methyl-1-methylene-4-phenyl-octahydronaphthalen-4*a*-ol (15*a*):** A solution of **7a**<sup>[2b]</sup> (18.5 mg, 0.0722 mmol) in toluene (15 mL) was purged with argon for 15 min and then heated in a microwave to 220 °C. After 1 h the reaction was concentrated. Purification by silica gel flash chromatography (2 → 5% ethyl acetate/hexanes) yielded **14a** (15.4 mg, 83%) as a white solid and **15a** (2.2 mg, 12%) as a colorless oil. For **14a**: M.p./b.p. 82.1–84.3 °C; <sup>1</sup>H NMR (500 MHz, CDCl<sub>3</sub>): δ = 7.28–7.21 (m, 5H), 4.97 (d, *J* = 1.5 Hz, 1H), 4.78 (s, 1H), 2.55 (dd, *J* = 12.9, 3.9 Hz, 1H), 2.43 (ddd, *J* = 12.9, 4.2, 2.4 Hz, 1H), 2.20 (ddd, *J* = 13.2, 13.2, 4.9 Hz, 1H), 2.10 (d, *J* = 12.0 Hz, 1H), 1.98 (dddd, *J* = 13.2, 13.2, 4.4 Hz, 1H), 1.92–1.87 (m, 1H), 1.80 (dddd, *J* = 12.7, 12.7, 12.0, 5.1 Hz, 1H), 1.76–1.71 (m, 1H), 1.60–1.56 (m, 2H), 1.47–1.41 (m, 2H), 1.34 (d, *J* = 1.2 Hz, 1H), 1.11 (d, *J* = 14.4 Hz, 1H), 1.00 ppm (d, *J* = 7.3 Hz, 3H); <sup>13</sup>C NMR (125 MHz, CDCl<sub>3</sub>): δ = 149.7, 142.3, 129.1, 127.9, 126.3 (2C), 108.7 (2C), 74.2, 55.3, 50.6, 41.6, 36.3, 31.2, 30.7, 27.0, 20.2, 18.7 ppm; IR (neat):  $\tilde{\nu}$  = 3553, 3084, 3061, 2988, 2934 cm<sup>-1</sup>; HRMS (EI): *m/z*: calcd for [*M*]<sup>+</sup>: 256.1827; found: 256.1839. For **15a**: <sup>1</sup>H NMR (500 MHz, CDCl<sub>3</sub>): δ = 7.39 (d, *J* = 7.3 Hz, 2H), 7.30–7.27 (m, 2H), 7.25–7.22 (m, 1H), 5.01 (d, *J* = 1.5 Hz, 1H), 4.77 (d, *J* = 1.5 Hz, 1H), 2.84 (dd, *J* = 5.9, 0.8 Hz, 1H), 2.63 (ddd, *J* = 13.7, 13.7, 4.6 Hz, 1H), 2.53 (dd, *J* = 10.0, 6.6 Hz, 1H), 2.32–2.19 (m, 2H), 1.91 (d, *J* = 1.7 Hz, 1H), 1.80–1.57 (m, 5H), 1.46 (ddd, *J* = 13.9, 3.2, 2.3 Hz, 1H), 0.83–0.75 (m, 1H), 0.72–0.67 (m, 1H), 0.71 ppm (d, *J* = 6.6 Hz, 3H); <sup>13</sup>C NMR (125 MHz, CDCl<sub>3</sub>): δ = 149.6, 144.2, 129.2 (2C), 128.3 (2C), 126.3, 109.7, 75.3, 53.1, 45.0, 44.3, 34.1, 32.6, 29.6, 28.0, 24.4, 22.1 ppm; IR (neat):  $\tilde{\nu}$  = 3476, 3023, 2928, 2866 cm<sup>-1</sup>; HRMS (EI): *m/z*: calcd for [*M*]<sup>+</sup>: 256.1827; found: 256.1819.

**(±)-(4*S*,4*aS*,6*R*,8*aS*)-6-Methyl-1-methylene-4-phenyl-octahydronaphthalen-4*a*-ol (17*a*):** Potassium bis(trimethylsilyl)amide (168 mg, 0.842 mmol) was added to a solution of **7a** (15.7 mg, 0.0612 mmol) in dimethoxyethane (1.5 mL) and toluene (0.5 mL). The reaction was heated to 85 °C for 1.5 h, cooled to ambient temperature and quenched with a saturated



aqueous solution of ammonium chloride. The aqueous phase was extracted three times with ethyl acetate and the combined organic layers were dried over magnesium sulfate, filtered and concentrated. Purification by silica gel flash chromatography (5% ethyl acetate/hexanes) yielded **13a** (9 mg, 57%) which was then re-dissolved in toluene (15 mL). After purging with argon for 15 min, the solution was heated to 220°C in a microwave for 30 min, cooled and concentrated. Purification by silica gel flash chromatography (2% ethyl acetate/hexanes) yielded **17a** (7.4 mg, 82%) as a white solid. For **13a**: M.p./b.p. 116–117°C; <sup>1</sup>H NMR (500 MHz, [D<sub>6</sub>]acetone): δ = 7.78–7.26 (m, 4H), 7.21–7.17 (m, 1H), 5.36 (d, *J* = 13.0 Hz, 1H), 3.72 (dd, *J* = 11.8, 1.6 Hz, 1H), 2.82–2.77 (m, 2H), 2.76–2.69 (m, 1H), 2.16–2.07 (m, 3H), 2.03–1.94 (m, 2H), 1.73–1.68 (m, 1H), 1.61 (dddd, *J* = 13.3, 3.6, 3.6, 1.9 Hz, 1H), 1.48 (s, 3H), 1.34–1.25 (m, 1H), 0.86 ppm (d, *J* = 7.1 Hz, 3H); <sup>13</sup>C NMR (125 MHz, [D<sub>6</sub>]acetone): δ = 206.7, 142.2, 139.2, 129.9 (2C), 129.1 (2C), 128.1, 127.8, 61.7, 53.1, 42.1, 39.1, 36.3, 30.0, 28.8, 25.6, 16.8 ppm; IR (neat):  $\tilde{\nu}$  = 2928, 2875, 2845, 1717 cm<sup>-1</sup>; HRMS (EI): *m/z*: calcd for [M]<sup>+</sup>: 256.1827; found: 256.1822.

For **17a**: M.p./b.p. 75.9–78.6°C; <sup>1</sup>H NMR (500 MHz, CDCl<sub>3</sub>): δ = 7.27–7.18 (m, 5H), 4.95 (d, *J* = 1.5 Hz, 1H), 4.74 (d, *J* = 1.0 Hz, 1H), 2.58 (dd, *J* = 12.9, 3.7 Hz, 1H), 2.44 (ddd, *J* = 12.9, 4.2, 2.4 Hz, 1H), 2.19 (ddd, *J* = 13.2, 13.2, 4.5 Hz, 1H), 2.07–2.03 (m, 1H), 2.00 (dddd, *J* = 13.2, 13.2, 13.2, 4.4 Hz, 1H), 1.80–1.69 (m, 2H), 1.62–1.54 (m, 3H), 1.40 (d, *J* = 1.2 Hz, 1H), 1.25 (ddd, *J* = 13.7, 3.7, 2.0 Hz, 1H), 0.97–0.89 (m, 1H), 0.86 (dd, *J* = 13.1, 12.5 Hz, 1H), 0.74 ppm (d, *J* = 6.6 Hz, 3H); <sup>13</sup>C NMR (125 MHz, CDCl<sub>3</sub>): δ = 149.5, 142.2, 127.9, 127.9 (2C), 126.3 (2C), 108.8, 73.6, 54.6, 49.6, 45.3, 36.4, 34.3, 31.0, 27.3, 24.1, 22.1 ppm; IR (neat):  $\tilde{\nu}$  = 3557, 3061, 2926, 2837, 1453 cm<sup>-1</sup>; HRMS (EI): *m/z*: calcd for [M]<sup>+</sup>: 256.1827; found 256.1804.

(±)-(4*R*,4*R*,8*R*,8*R*)-6,6-Dimethyl-1-methylene-4-phenyl-octahydronaphthalen-4a-ol (**14d**): Potassium bis(trimethylsilyl)amide (168 mg, 0.842 mmol) was added to a solution of (–)-**7d**<sup>[3]</sup> (45.7 mg, 0.169 mmol) in dimethoxyethane (3 mL) and toluene (1.5 mL). The reaction was heated to 85°C for 1.5 h, cooled to ambient temperature and quenched with a saturated aqueous solution of ammonium chloride. The aqueous phase was extracted three times with ethyl acetate and the combined organic layers were dried over magnesium sulfate, filtered and concentrated. Purification by silica gel flash chromatography (5% ethyl acetate/hexanes) gave **13d** (36 mg, 78%) as a white solid. A solution of **13d** (11.0 mg, 0.0407 mmol) in toluene (15 mL) was purged with argon for 15 min and then heated in a microwave to 220°C. After 1 h the reaction was concentrated. A <sup>1</sup>H NMR of the crude material confirmed the presence of a single isomer. Purification by silica gel flash chromatography (8% ethyl acetate/hexanes) yielded **14d** (10.9 mg, 99%) as a white solid. For **13d**: M.p./b.p. 99.4–101.2°C; <sup>1</sup>H NMR (500 MHz, [D<sub>6</sub>]acetone): δ = 7.30–7.18 (m, 5H), 5.63 (s, br, 1H), 3.72 (d, *J* = 11.6 Hz, 1H), 2.96 (d, br, *J* = 17.4 Hz, 1H), 2.75 (dddd, *J* = 13.0, 13.0, 13.0, 3.5 Hz, 1H), 2.23–2.20 (m, 1H), 2.16–1.96 (m, 5H), 1.62 (d, *J* = 13.4 Hz, 1H), 1.55 (s, 3H), 1.16–1.09 (m, 1H), 1.06 (s, 3H), 0.90 ppm (s, 3H); <sup>13</sup>C NMR (75 MHz, [D<sub>6</sub>]acetone): broad signals due to interchanging conformers prevented all peaks from being detected. High-temperature NMR to resolve the conformers was impossible due to the resulting carbonyl ene reaction; IR (neat):  $\tilde{\nu}$  = 2952, 2926, 1698 cm<sup>-1</sup>; HRMS (EI): *m/z*: calcd for [M]<sup>+</sup>: 270.1984; found 270.2042. For **14d**: Spectral data for this compound was in agreement with reported previously.<sup>[3]</sup>

(±)-(E,2*S*,9*S*)-2-(4-Methoxybenzyl)-5,9-dimethyl-2-phenylcyclodec-5-enone (**17aa**): A solution of **7a** (56.1 mg, 0.219 mmol) in DME (4 mL) was treated with a solution of KHMDS (131.0 mg, 0.657 mmol) in DME (3 mL). The resulting cloudy yellow solution was plunged into a pre-warmed oil bath and heated at 85°C for 15 min whereupon it turned clear orange. This mixture was cooled to room temperature, then immediately to –78°C after which it was treated with PMBCl (0.06 mL, 0.443 mmol). The reaction was stirred for a further 15 min and then it was quenched with water and warmed to room temperature. The layers were separated and the aqueous phase was extracted with Et<sub>2</sub>O (3 × 20 mL). The organic layers were combined, dried over MgSO<sub>4</sub>, filtered

and concentrated. The product was isolated by flash chromatography in 10% EtOAc/hexanes, affording ketone **13aa** (37.7 mg, 0.100 mmol, 46%) as a yellow oil. **13aa** was dissolved in toluene (13 mL), purged with argon for 15 min and then heated in a microwave to 200°C for 80 min. Upon cooling, the reaction mixture was concentrated to give a yellow oil. The product was recovered by flash chromatography in 10% EtOAc/hexanes, affording **17aa** (18.5 mg, 0.0491 mmol, 49%) as a white solid. M.p./b.p. 61–62°C; <sup>1</sup>H NMR (500 MHz, [D<sub>6</sub>]acetone): δ = 7.62 (d, *J* = 7.4 Hz, 2H), 7.33 (dd, *J* = 7.7, 7.7 Hz, 2H), 7.24–7.20 (m, 1H), 6.88 (d, *J* = 8.7 Hz, 2H), 6.61 (d, *J* = 8.8 Hz, 2H), 4.81 (d, *J* = 1.4 Hz, 1H), 4.61 (d, *J* = 0.7 Hz, 1H), 3.76 (d, *J*<sub>AB</sub> = 15.0 Hz, 1H), 3.67 (s, 3H), 3.37 (d, *J*<sub>AB</sub> = 15.0 Hz, 1H), 2.66–2.52 (m, 3H), 2.15–2.12 (m, 1H), 1.98–1.96 (m, 1H), 1.74–1.58 (m, 5H), 1.46–1.39 (m, 2H), 1.06–0.93 (m, 1H), 0.83 ppm (d, *J* = 6.4 Hz, 3H); <sup>13</sup>C NMR (100 MHz, [D<sub>6</sub>]acetone): δ = 158.9, 151.0, 143.4, 131.9, 131.9 (2C), 131.4 (2C), 128.0 (2C), 126.9, 114.0 (2C), 107.7, 77.7, 55.4, 51.8, 44.9, 42.0, 36.1, 35.5, 33.2, 30.4, 28.4, 26.1, 23.1 ppm; IR (neat):  $\tilde{\nu}$  = 3559, 2948, 2847 cm<sup>-1</sup>; HRMS (EI): *m/z*: calcd for [M]<sup>+</sup>: 376.2402; found 376.2395.

## Acknowledgements

We thank the Natural Science and Engineering Research Council of Canada (NSERC), Merck-Frosst Canada, Merck Co., and Boehringer Ingelheim for generous funding. L. B. thanks the University of Ottawa for a University Research Chair. T.W. thanks the Canada Research Chairs Program. E.L.O.S., S.A. and J.H. thank the NSERC for post-graduate scholarships (PGS-D).

- [1] E. L. O. Sauer, J. Hooper, T. Woo, L. Barriault, *J. Am. Chem. Soc.* **2007**, *129*, 2112.
- [2] a) S. Arns, L. Barriault, *Chem. Commun.* **2007**, 2211; b) E. L. O. Sauer, L. Barriault, *J. Am. Chem. Soc.* **2004**, *126*, 8569; c) S. Arns, L. Barriault, *J. Org. Chem.* **2006**, *71*, 1809.
- [3] D. Gauvreau, L. Barriault, *J. Org. Chem.* **2005**, *70*, 8840.
- [4] S. Arns, I. Denissova, M.-E. Lebrun, C. M. Grisé, L. Barriault, *J. Org. Chem.* **2007**, *72*, 9314.
- [5] W. Kohn, L. A. Sham, *Phys. Rev. A* **1965**, *10*, 1133.
- [6] a) C. Lee, W. Yang, R. G. Parr, *Phys. Rev. B* **1988**, *37*, 785; b) A. D. Becke, *J. Chem. Phys.* **1993**, *98*, 5648.
- [7] Jaguar 6.0, Schrödinger LLC, Portland, **2005**.
- [8] Spartan 02, Wavefunction Inc., Irvine, **2002**.
- [9] J. J. P. Stewart, *Comput. Chem.* **1989**, *10*, 209.
- [10] D. J. Tannor, B. Marten, R. Murphy, R. A. Friesner, D. Sitkoff, A. Nicholls, M. Ringnalda, W. A. Goddard III, B. Honig, *J. Am. Chem. Soc.* **1994**, *116*, 11875.
- [11] CPMD, Version 3.13.2, IBM Research Division and MPI für Festkörperforschung, Stuttgart, **2008**.
- [12] J. P. Perdew, K. Burke, M. Ernzerhof, *Phys. Rev. Lett.* **1996**, *77*, 3865.
- [13] a) N. Troullier, J. L. Martins, *Phys. Rev. B* **1991**, *43*, 1993; b) L. Kleinman, D. M. Bylander, *Phys. Rev. Lett.* **1982**, *48*, 1425.
- [14] The counterion was not included since the anionic species but could reasonably be assumed to increase the energy barrier for the ring inversion.
- [15] A. E. Reed, L. A. Curtiss, F. Weinhold, *Chem. Rev.* **1988**, *88*, 899.
- [16] a) A. Rauk, J. D. Andose, W. G. Frick, R. Tang, K. Mislow, *J. Am. Chem. Soc.* **1971**, *93*, 6507; b) G. B. Ellison, P. C. Engelking, W. C. Lineberger, *J. Am. Chem. Soc.* **1978**, *100*, 2556; c) P. R. Peoples, J. B. Grutzner, *J. Am. Chem. Soc.* **1980**, *102*, 4709.

Received: May 13, 2010  
Published online: October 18, 2010